

## **SUPPLEMENTARY MATERIAL**

Halperin et al.

### **Supplemental Movie S1**

Live-cell imaging over 42 hours of WT and PB2 KO D6 cells labeled with NucSpot, SPY-tubulin, and SPY-actin.

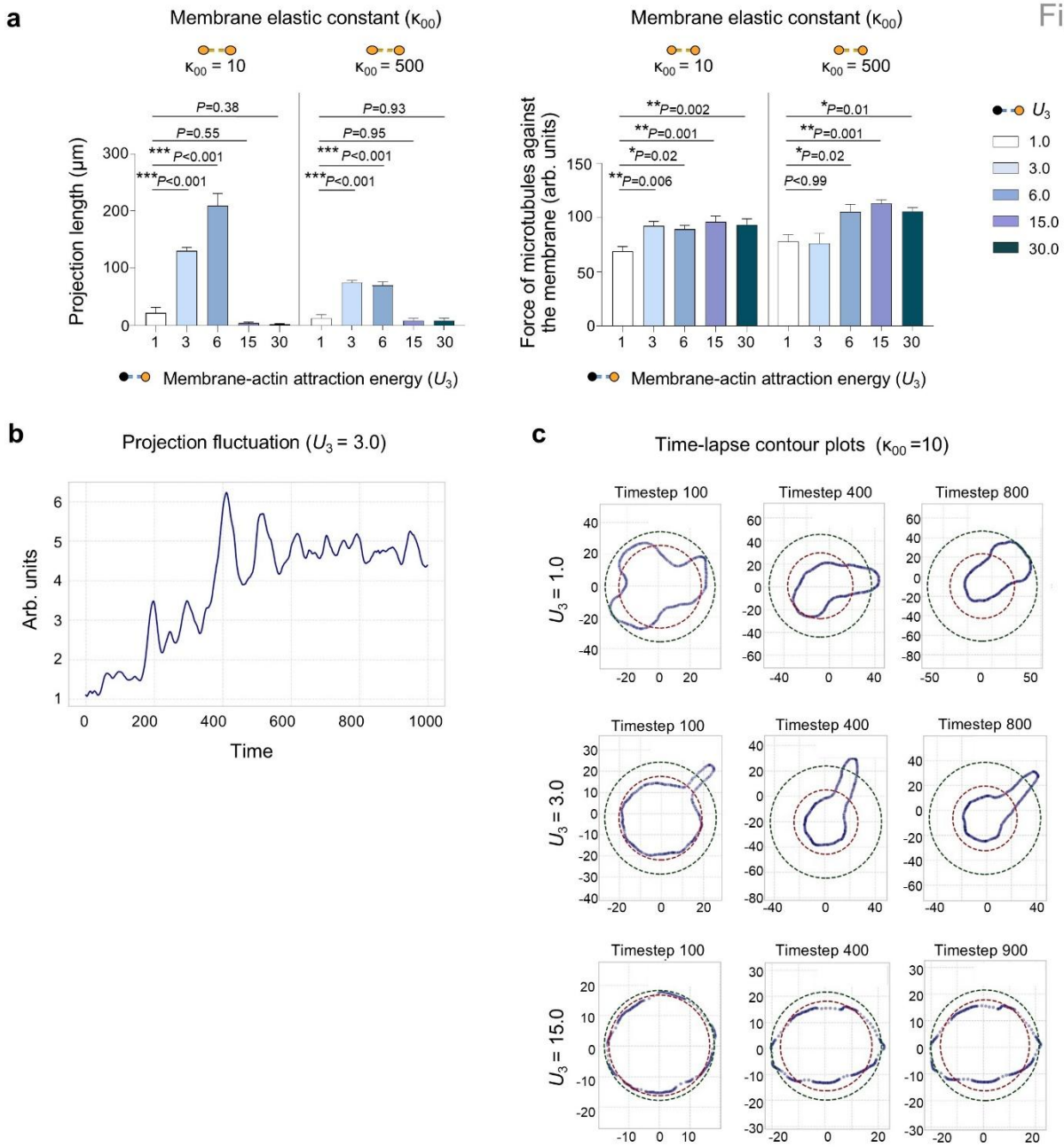
### **Supplemental Figures S1 - S8.**

See pages below.

### **Supplemental Table S1.**

Overview of cell numbers in single nucleus RNA sequencing samples after quality filtering.

Fig. S1

**Figure S1. Molecular dynamics modeling of cortical actin tension during neurodifferentiation.**

**a)** Simulated neurite projection area (left) and microtubule pushing force (right) under two membrane elastic constants ( $\kappa_{00} = 10$  vs.  $500$ ) and varying membrane-cytoskeleton attraction energies ( $U_3$ ). At low membrane tension ( $\kappa_{00} = 10$ ), projection area increases markedly at moderate  $U_3$  values, indicating that soft membranes favor neurite protrusion. Extremely low  $U_3$  values impaired projection stability, reflecting insufficient actin-membrane coupling. At high membrane tension ( $\kappa_{00} = 500$ ), projections were suppressed across all  $U_3$  conditions. Microtubule pushing force remained largely unchanged.

Bar graphs (for projection length and force against membrane) represent mean  $\pm$  SEM, one-way ANOVA with Dunnett's multiple-comparison test.

**b)** Time-course analysis of projection length at moderate  $U_3$  (3.0) with low membrane tension ( $\kappa_{00} = 10$ ) shows dynamic fluctuations of extensions, consistent with active and flexible membrane states that promote neurite protrusion.

**c)** Simulated cell shape dynamics under varying  $U_3$  values with constant membrane tension ( $\kappa_{00} = 10$ ). Contour plots show evolving cell boundaries (blue) at selected time points, with dashed red (nuclear center) and green (cellular boundary) reference circles. At  $U_3 = 3.0$ , cells formed a stable polarized projection with nuclear compaction and displacement, mimicking early neurite emergence. Low  $U_3$  (1.0) yielded unstable morphologies without clear axis formation, while high  $U_3$  (15.0) constrained cells to near-spherical shapes with minimal protrusion. These results suggest that balanced actin-membrane coupling and cortical tension are critical for stable, directed neurite initiation.

Fig. S2

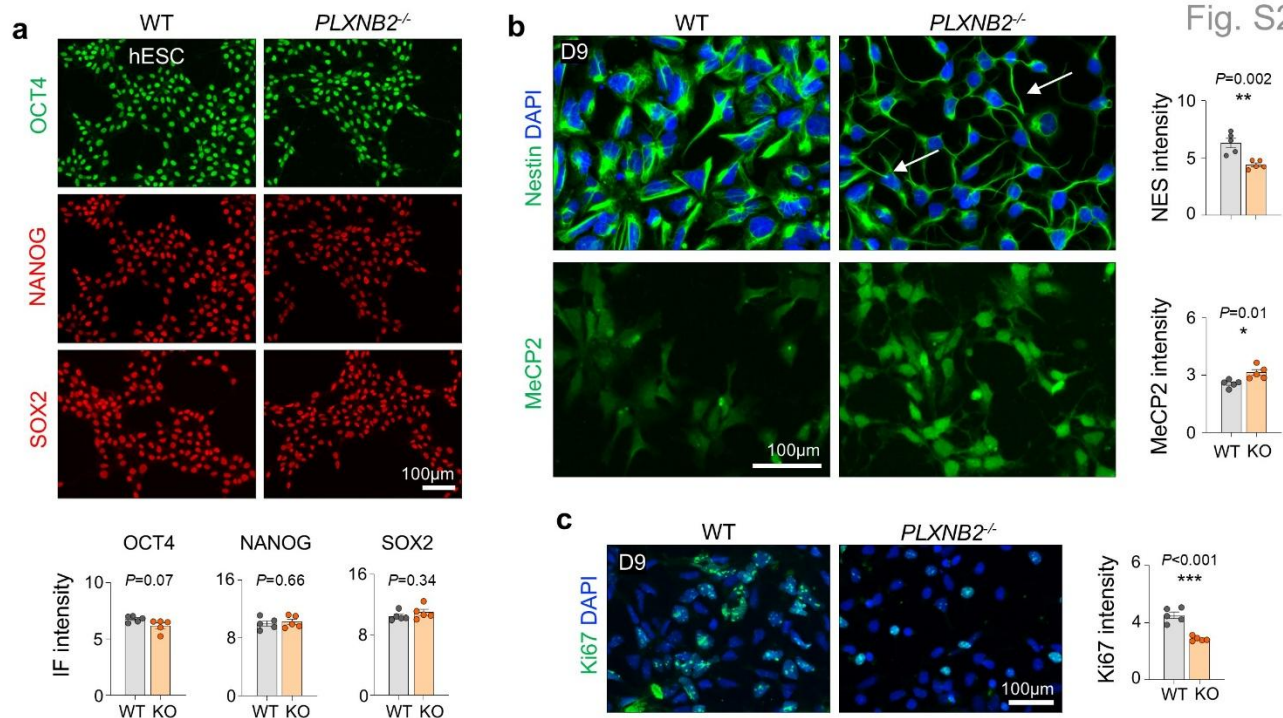


**Figure S2. Plexin-B2 KO cells display early neuronal lineage commitment.**

**a)** IF demonstrates comparable expression of pluripotency markers in WT and *PLXNB2*<sup>-/-</sup> hESCs.

**b)** IF shows reduced Nestin and increased MeCP2 expression in D9 *PLXNB2*<sup>-/-</sup> cells relative to WT. KO cells also displayed morphological changes with elongated protrusions (arrows), a sign of premature neuronal differentiation.

**c)** IF for proliferation marker Ki67 reveals reduced proliferative activity in D9 *PLXNB2*<sup>-/-</sup> cultures. Quantification based on n = 5 fields (each averaged from ~50 cells per field) for each condition, two-tailed nested t-test. Bar graphs represent mean  $\pm$  SEM.

Fig. S3

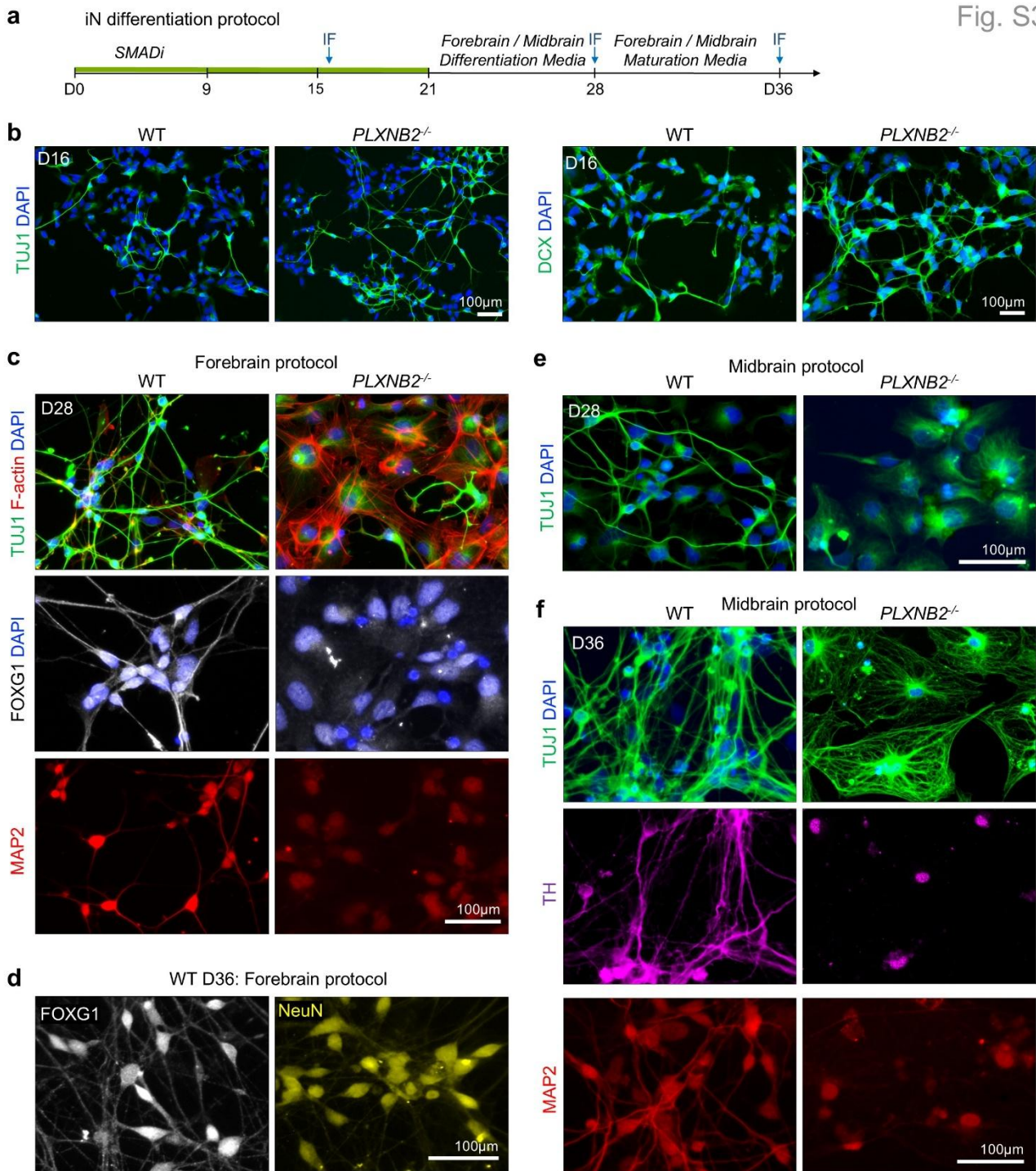


**Figure S3. Lineage instability in *PLXNB2*<sup>-/-</sup> cells under mismatched media conditions.**

**a)** Timeline of forebrain or midbrain differentiation protocols for iNs.

**b)** IF at D16 of iN protocol shows denser networks of DCX<sup>+</sup> or TUJ1<sup>+</sup> neurite projections in *PLXNB2*<sup>-/-</sup> cells as compared with WT cells.

- c) At D28 of forebrain differentiation protocol, *PLXNB2*<sup>-/-</sup> cells display aberrant morphology and loss of stable neuronal marker gene expression, in contrast to WT cells that displayed organized TUJ1<sup>+</sup> and MAP2<sup>+</sup> neuronal networks and expression of forebrain marker FOXG1.
- d) WT D36 iNs from the forebrain protocol show expression of NeuN and forebrain marker FOXG1.
- e) At D28 of midbrain differentiation protocol, WT cells maintained organized TUJ1<sup>+</sup> neuronal networks, but *PLXNB2*<sup>-/-</sup> cells have acquired an aberrant morphology.
- f) WT D36 cells treated with midbrain maturation media. *PLXNB2*<sup>-/-</sup> cells show loss of organized TUJ1 and MAP2 networks and lack expression of midbrain marker tyrosine hydroxylase (TH).

Fig. S4

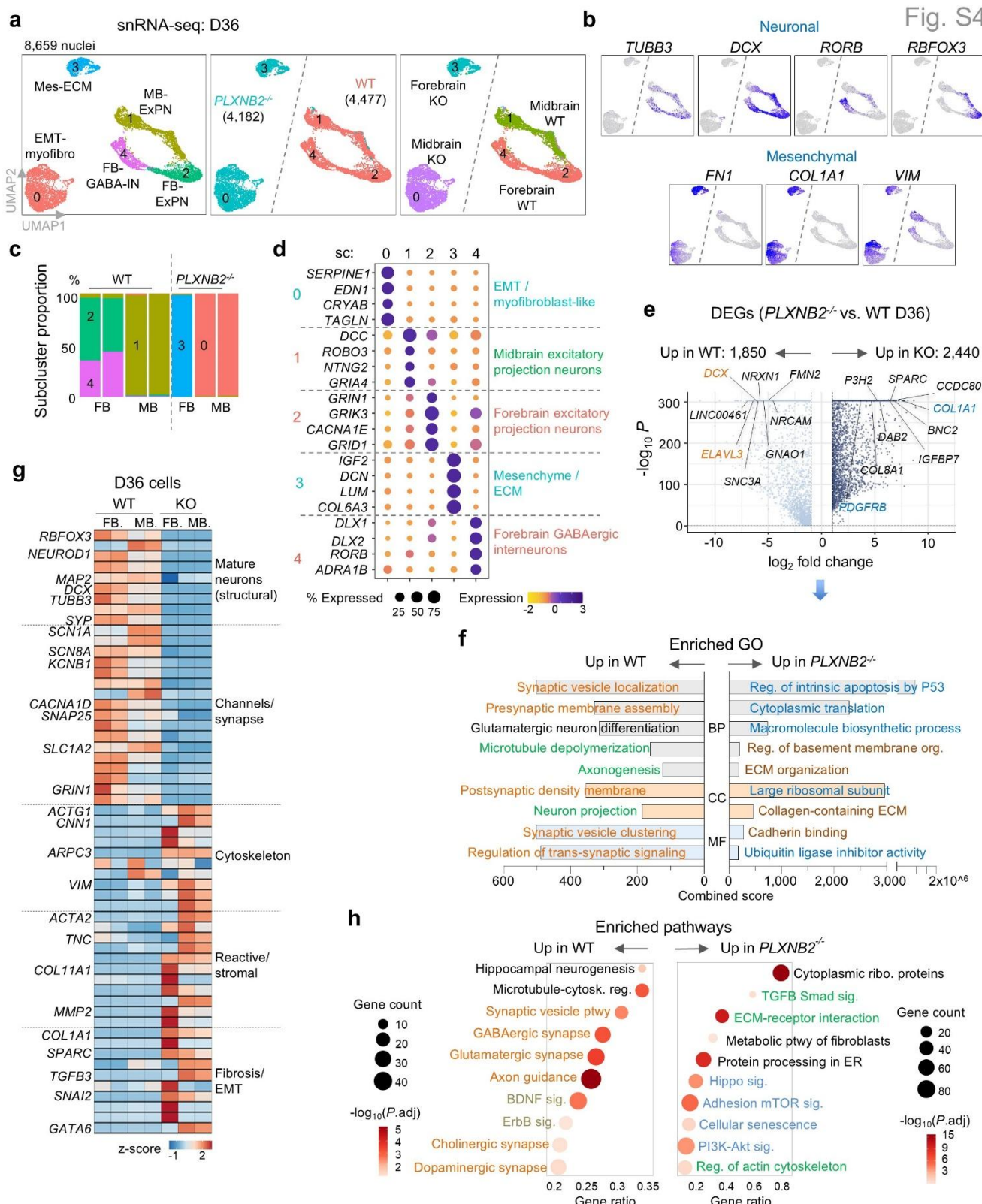


Figure S4. Mismatched extrinsic cues lead to lineage instability.

a) UMAP embedding of snRNA-seq data of D36 cells reveals major cell populations separated by

genotype and by forebrain (FB) versus midbrain (MB) differentiation protocols.

- b)** Feature plots showing expression of representative marker genes for subclusters.
- c)** Stacked bar graphs showing relative proportions of subclusters in D36 WT and *PLXNB2*<sup>-/-</sup> cells across both FB and MB differentiation protocols. Graphs derived from seven combined snRNA-seq samples (two WT-FB, two WT-MB, and one KO-FB and two KO-MB).
- d)** Dot plot showing expression of marker genes in subclusters of D36 cells, with major themes annotated on the right and color-coded according to genotypes and FB vs. MB protocols.
- e)** Volcano plot of differentially expressed genes (DEGs) in *PLXNB2*<sup>-/-</sup> versus WT cells (pooled across FB and MB protocols), with top genes highlighted.
- f)** Gene ontology (GO) enrichment analysis of DEGs, grouped by biological process (BP), cellular component (CC), and molecular function (MF), color-coded by theme.
- g)** Heatmap of selected DEGs grouped by function in D36 WT and *PLXNB2*<sup>-/-</sup> cells cultured with FB or MB protocols.
- h)** Bubble plot showing enriched pathways upregulated in D36 *PLXNB2*<sup>-/-</sup> versus WT cells.

Fig. S5

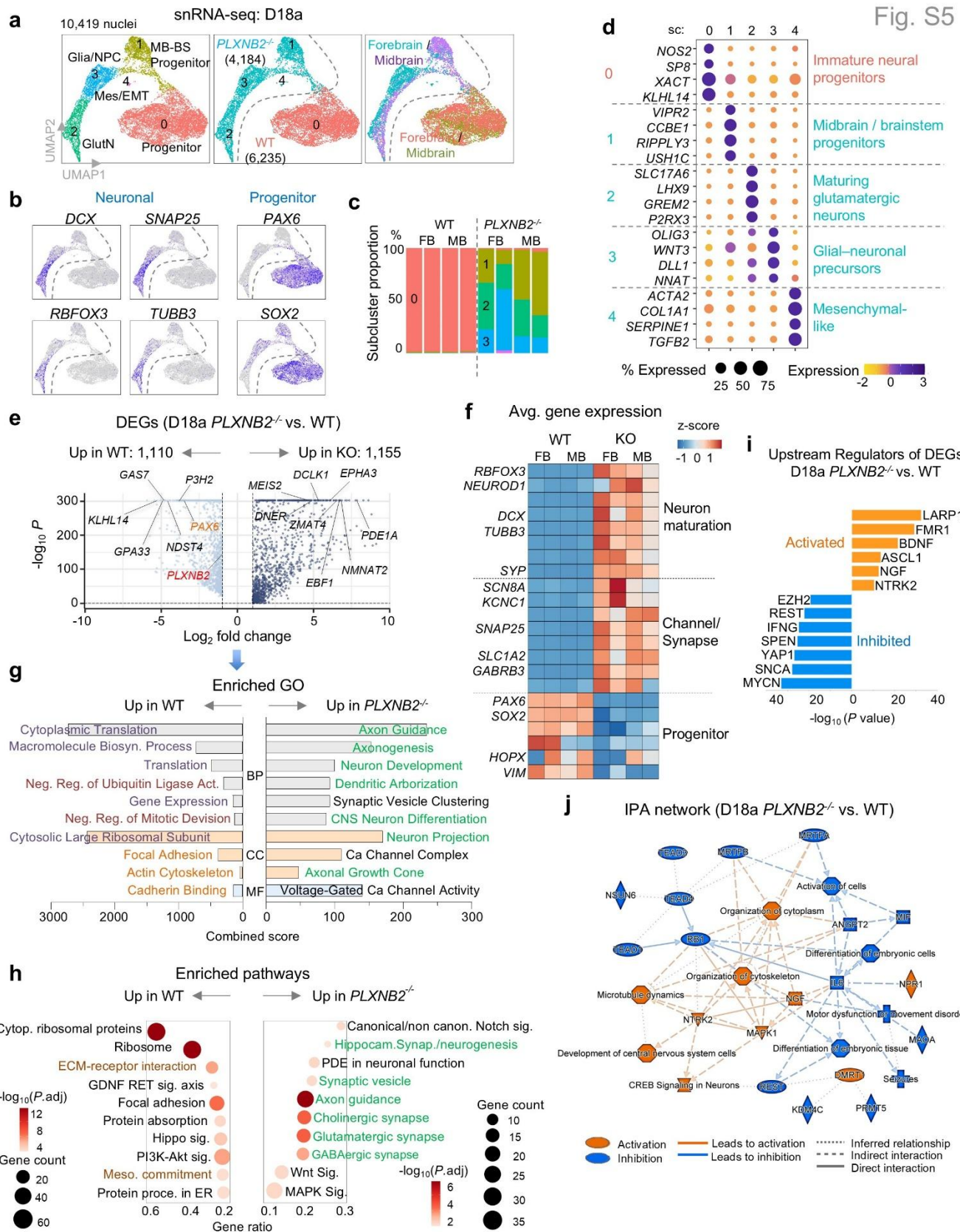


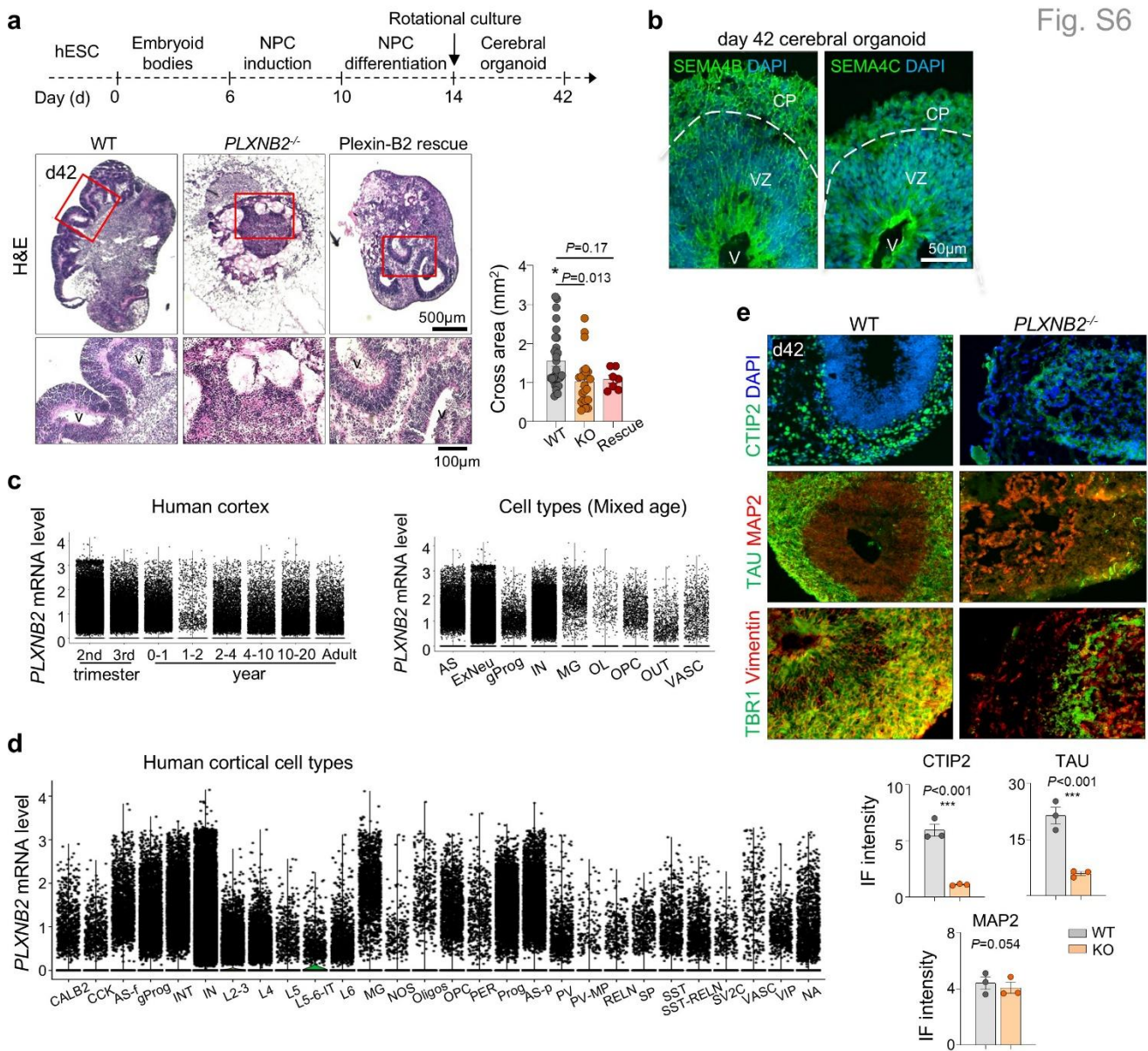
**Figure S5. Accelerated maturation cues stabilize neuronal lineage of PLXNB2<sup>-/-</sup> iNs.**

**a)** UMAP embedding of D18a cells under the accelerated protocol (switch to maturation media after the

first passage at D9). WT cells (forebrain and midbrain protocols) clustered together as sc-0, whereas *PLXNB2*<sup>-/-</sup> cells segregated into four distinct subclusters.

- b)** Feature plots showing expression of representative marker genes of each subcluster.
- c)** Bar graphs illustrating distinct cell type proportions for WT and *PLXNB2*<sup>-/-</sup> cells under forebrain (FB) or midbrain (MB) iN protocols.
- d)** Dot plot of marker gene expression across subclusters of D18a cells.
- e)** Volcano plot of DEGs (*PLXNB2*<sup>-/-</sup> vs. WT) at D18a (pooled across FB and MB protocols), with top DEGs labeled.
- f)** Heatmap of representative DEGs grouped by functional categories, comparing WT and *PLXNB2*<sup>+/+</sup> cells under FB and MB protocols.
- g)** GO enrichment analysis of DEGs, grouped into biological process (BP), cellular component (CC), and molecular function (MF) categories, color-coded by theme.
- h)** Bubble plot showing pathways significantly enriched in *PLXNB2*<sup>+/+</sup> versus WT cells.
- i)** Upstream regulator analysis predicts activation of neuronal regulators (BDNF, ASCL1, NGF) and inhibition of progenitor regulators (REST, EZH2, YAP1) in *PLXNB2*<sup>+/+</sup> D18a cells.
- j)** IPA network analysis of *PLXNB2*<sup>+/+</sup> versus WT cells at D18a reveals activation of cytoskeletal remodeling, CREB signaling, and neuronal development, alongside suppression of progenitor maintenance and proliferation pathways.

Fig. S6

**Figure S6. Plexin-B2 is required for cortical structure during neurogenesis.**

**a)** Top, schematic of the cerebral organoid protocol. Bottom, H&E staining (enlarged images at bottom panel) showing that WT organoid at day 42 contained organized cortical architecture with ventricle-like (V) structures surrounded by ventricular zone (VZ) and cortical plate (CP). In contrast, *PLXNB2*<sup>-/-</sup> organoids displayed aberrant cystic morphology lacking VZ organization. Re-expression of Plexin-B2 rescued the KO phenotype. Quantification of organoid cross-sectional area, n = 6-14 organoids per group, one-way ANOVA with Dunnett's multiple comparisons test. Bar graphs show mean  $\pm$  SEM.

**b)** Expression of SEMA4B and SEMA4C, cognate Plexin-B2 ligands, in d42 WT cerebral organoids.

DAPI used for nuclear counterstaining.

- c) Left, temporal *PLXNB2* expression levels across developmental stages in human cortex. Right, *PLXNB2* expression across major cortical cell classes, including astrocytes (AS), excitatory neurons (ExNeu), glial progenitors (gProg), interneurons (IN), microglia (MG), oligodendrocytes (OL), oligodendrocyte progenitor cells (OPC), outer radial glia (oRG), and vascular cells (VASC). Based on data from Velmeshev et al., 2023.
- d) Expression of *PLXNB2* in defined neuronal and non-neuronal subtypes of the developing human cortex, including excitatory neurons (L2–L6, L5–6 IT), inhibitory neuron classes (PV, SST, VIP), radial glia, astrocyte populations (AS-f, AS-p), microglia (MG), oligodendroglia (OPC, OL), and non-neuronal populations (VASC, NOS, NA). Based on data from Velmeshev et al., 2023.
- e) *PLXNB2*<sup>-/-</sup> d42 organoids contained fewer CTIP2<sup>+</sup> deep-layer cortical neurons, which were arranged in disorganized manner. Additional markers MAP2 (dendrite marker), TAU (axon marker), vimentin (radial glial scaffold marker), and TBR1 (layer VI cortical neuron marker) reveal disrupted cortical lamination in *PLXNB2*-deficient organoids. Quantification based on n = 3 independent organoids per condition, with ~30 fields of view analyzed per organoid. Bar graphs represent mean ± SEM; two-tailed nested t-test.

Fig. S7

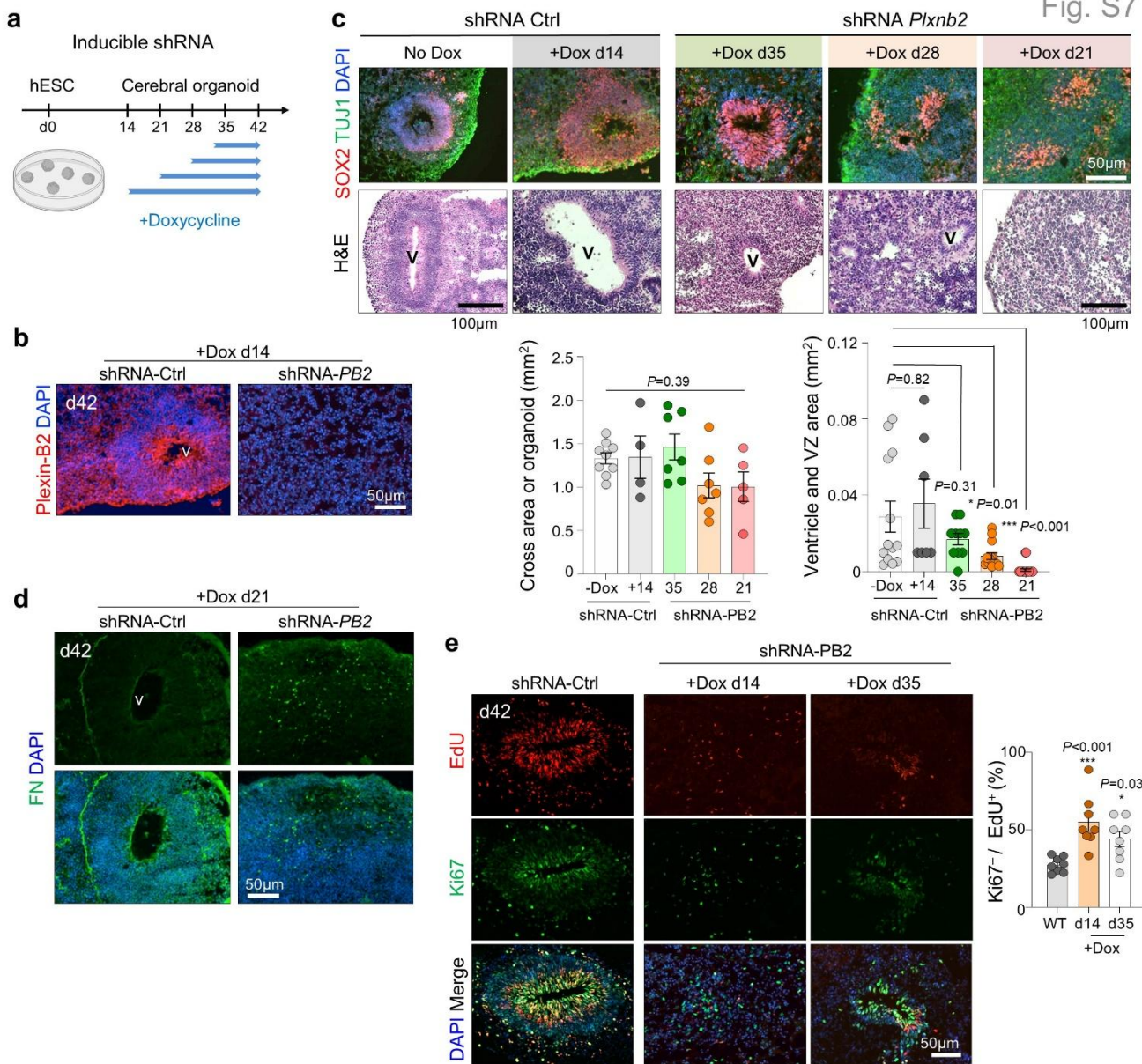


**Figure S7. *PLXNB2* deficiency disrupts cerebral organoid development.**

**a)** Experimental scheme of doxycycline (Dox)-inducible *PLXNB2* shRNA knockdown (KD) initiated at different timepoints.

**b)** IF confirming loss of Plexin-B2 protein expression in d42 cerebral organoids after KD induction at day 14.

**c)** Temporal KD analysis showing that earlier KD (day 21) caused more severe structural disorganization compared to KD at later stages. IF for SOX2 (progenitors) and TUJ1 (neurons), together with H&E staining, demonstrate progressive loss of ventricular morphology and progenitor zone integrity. n = 4-6.

12 organoids per group, with two randomly selected regions per organoid. One-way ANOVA with Dunnett's post hoc test. Bar graphs show mean  $\pm$  SEM.

- d)** IF for fibronectin (FN) at d42 showing disruption of the FN network and abnormal ventricle-like structures in *PLXNB2* KD organoids.
- e)** Pulse-chase proliferation assay in *PLXNB2* KD cerebral organoids with EdU and Ki67 staining. Both early (d14) and later (d35) KD led to disrupted ventricular morphology and premature cell cycle exit, with earlier KD causing a more severe phenotype. n = 8 organoids per group, with two randomly selected regions per organoid. One-way ANOVA with Dunnett's multiple comparisons test. Bar graphs show mean  $\pm$  SEM.

Fig. S8

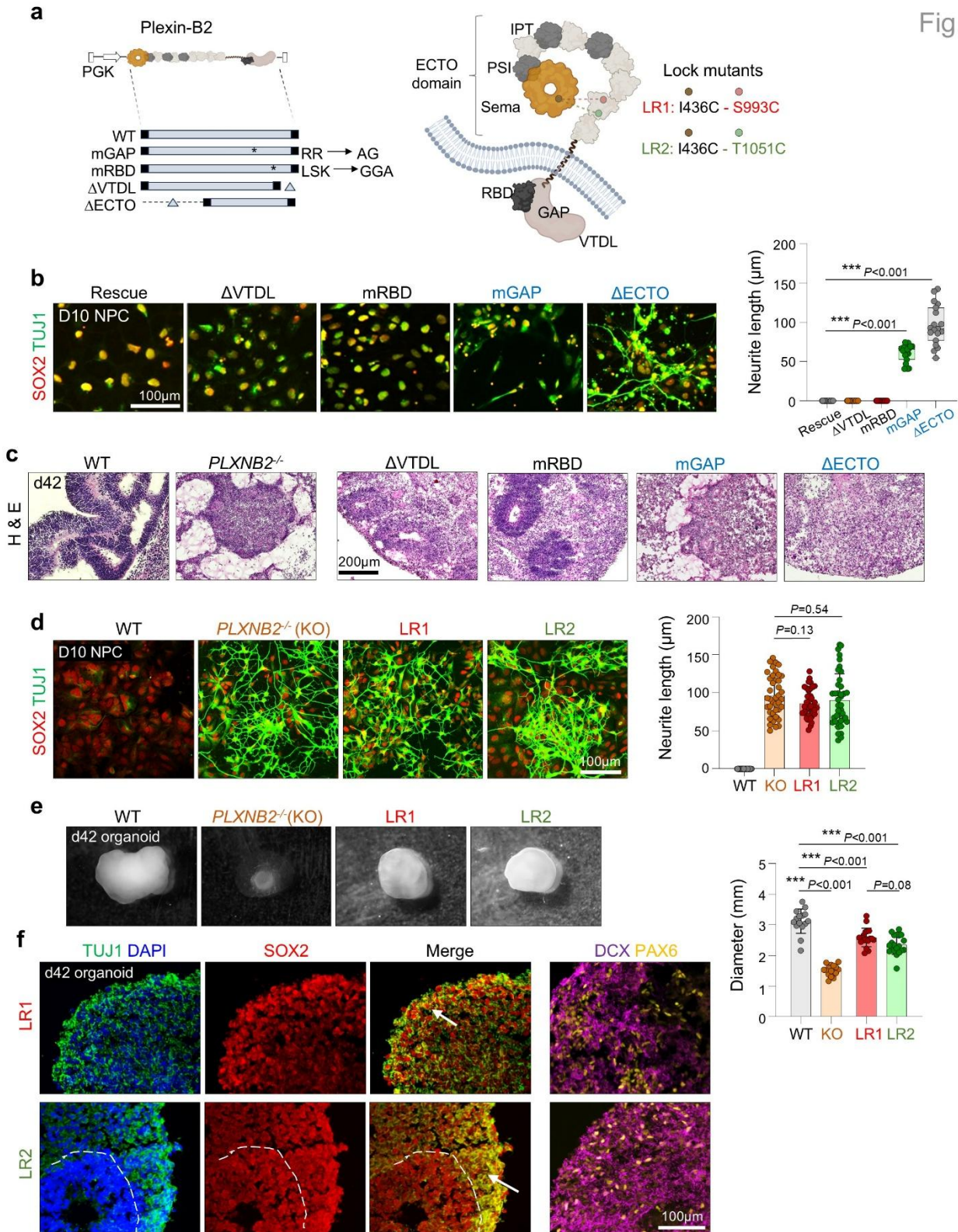


**Figure S8. Plexin-B2 mutational analysis reveals critical domains for gating neuronal differentiation.**

**a)** Left, mutations in specific functional domains of Plexin-B2. mGAP: mutated GTPase activating

protein domain; mRBD: mutated Rho binding domain;  $\Delta$ VTDL: deleted VTDL PDZ-binding motif at C-terminus;  $\Delta$ ECTO: deleted extracellular domain. Right: cartoon model indicating arrangement of Plexin-B2 domains. LR1 and LR2 indicated the “locked ring” mutations designed to prevent bending of the ECTO domain ring by mechanical stimuli.

- b)** Rescue experiments show that at D10 of iN protocol, mGAP and  $\Delta$ ECTO mutations failed to rescue the premature differentiation phenotype of Plexin-B2 KO. n=18 fields for each condition. One-way ANOVA with Dunnett’s post hoc test. Box plots show median and quartiles.
- c)** Cerebral organoids carrying different domain-specific mutations of Plexin-B2 at day 42.
- d)** IF images of D10 cells in rescue experiments show that the locked ring mutations LR1 and LR2 phenocopy Plexin-B2 KO. n = 40 neurons for each condition. One-way ANOVA with Dunnett’s post hoc test. Bar graphs show mean  $\pm$  SEM.
- e)** Cerebral organoids derived from *PLXNB2*<sup>-/-</sup> or LR1 or LR2 mutant hESCs showed reduced size. Each data point represents one organoid (n = ~20 organoids per group). One-way ANOVA with Dunnett’s multiple comparisons test. Bar graphs show mean  $\pm$  SEM.
- f)** Cerebral organoids from LR1 or LR2 mutant hESCs at d42 show SOX2<sup>+</sup> progenitor cells overlapping with TUJ1<sup>+</sup> neurons (arrows), and disorganization of PAX6<sup>+</sup> and DCX<sup>+</sup> populations.

**Table S1. Overview of single nucleus RNA sequencing samples.**

Protocol	Day of culture	Sample ID	Cell numbers (post-QC)
<b>Induced neurons</b>	<b>D9</b>	WT-1	889
		WT-2	2,595
		WT-3	1,490
			<i>total 4,974</i>
		KO-1	564
		KO-2	1,007
		KO-3	1,255
			<i>total 2,826</i>

<b>Induced neurons</b>	<b>D36</b>	WT1 - Forebrain	1,339
		WT2 - Forebrain	1,173
		WT1 - Midbrain	960
		WT2 - Midbrain	1,005
			<i>total 4,477</i>
		KO1 - Forebrain	1,027
		KO1 - Midbrain	1,489
		KO2 - Midbrain	1,666
			<i>total 4,182</i>

<b>Induced neurons -</b>	<b>D18a</b>	WT1 - Forebrain	1,890
<b>Accelerated protocol</b>		WT2 - Forebrain	1,525
		WT1 - Midbrain	1,451
		WT2 - Midbrain	1,369
			<i>total 6,235</i>
		KO1 - Forebrain	632
		KO2 - Forebrain	1,273
		KO1 - Midbrain	1,341
		KO2 - Midbrain	938
			<i>total 4,184</i>

<b>Cerebral organoid</b>	<b>d42</b>	WT-1	2,600
		WT-2	3,181
		WT-3	2,141
			<i>total 7,922</i>
		KO-1	4,955
		KO-2	211
		KO-3	1,853
			<i>total 7,019</i>